Soft Matter

Combined Description of Pressure-Volume-Temperature and Dielectric Relaxation of Several Polymeric and Low-Molecular-Weight Organic Glass-Formers using "SL-TS2" Mean-Field Approach

Journal:	*Soft Matter*
Manuscript ID	SM-ART-08-2022-001049.R2
Article Type:	Paper
Date Submitted by the Author:	25-Oct-2022
Complete List of Authors:	Ginzburg, Valeriy; Michigan State University, Chemical Engineering and Materials Science Zaccone, Alessio; University of Milan, Physics; University of Cambridge, Chemical Engineering and Biotechnology Casalini, Riccardo; Naval Research Laboratory, Chemistry Division

Combined Description of Pressure-Volume-Temperature and Dielectric Relaxation of Several Polymeric and Low-Molecular-Weight Organic Glass-Formers using SL-TS2 Approach†

Valeriy V. Ginzburg[1,*], Alessio Zaccone[2], and Riccardo Casalini[3]

[1]Department of Chemical Engineering and Materials Science, Michigan State University, East Lansing, MI 48824, USA

[2]University of Milan, Department of Physics, via Celoria 16, 20133 Milano, Italy

[3]Chemistry Division, Naval Research Laboratory, 4555 Overlook Avenue SW, Washington DC 20375, USA

*Corresponding author, email vvg851966@gmail.com

†Electronic supporting information (ESI) available, see…

Abstract

We apply our recently-developed mean-field "SL-TS2" (two-state Sanchez-Lacombe) model to simultaneously describe dielectric α-relaxation time, τ_α, and pressure-volume-temperature (PVT) data in four polymers (polystyrene, poly(methylmethacrylate), poly(vinyl acetate) and poly(cyclohexane methyl acrylate)) and four organic molecular glass formers (ortho-terphenyl, glycerol, PCB-62, and PDE). Previously, it has been shown that for all eight materials, the Casalini-Roland thermodynamical scaling, $\tau_\alpha = f(Tv_{sp}^{\gamma})$ (where T is temperature and v_{sp} is specific volume) is satisfied (Casalini, R.; Roland, C. M. *Phys. Rev. E* **2004**, *69*(6), 062501). It has also been previously shown that the same scaling emerges naturally (for sufficiently low pressures) within the "SL-TS2" framework (Ginzburg, V. V. *Soft Matter* **2021**, *17*, 9094–9106.) Here, we fit the ambient pressure curves for the relaxation time and the specific volume as functions of temperature for the eight materials and observe a good agreement between theory and experiment. We then use the Casalini-Roland scaling to convert those results into "master curves", thus enabling predictions of relaxation times and specific volumes at elevated pressures. The proposed approach can be used to describe other glass-forming materials, both low-molecular-weight and polymeric.

Introduction

Glass transition is an important phenomenon impacting multiple properties of amorphous materials (mechanical, transport, thermophysical, etc.).[1–6] In particular, as a material approaches its glass transition from the higher-temperature, liquid state, its viscosity and characteristic relaxation time increase multiple orders of magnitude, while its coefficient of thermal expansion (CTE) and heat capacity change abruptly (nearly discontinuously).[1,3,7–11] The glass transition temperature (T_g) depends on the molecular structure of the material and the applied pressure; it is also a weak function of the rate of temperature change (heating or cooling).

Over the past century, theoretical understanding of the glass transition has advanced significantly. The earliest models (Vogel,[12] Fulcher,[13] Tammann and Hesse[14]) described the viscosity or relaxation time as functions of temperature diverging at some finite temperature T_0 ($0 < T_0 < T_g$). The Vogel-Fulcher-Tammann-Hesse (VFTH) model – and the effectively equivalent Williams-Landel-Ferry[15] (WLF) equation – was subsequently explained theoretically on the basis of "free volume" (Doolittle[16]) or "configurational entropy" (Adam and Gibbs [AG][17]). Other well-known empirical and semi-phenomenological models for the relaxation time as a function of temperature included MYEGA,[18] KSZ,[19] Avramov-Michev,[20] Elmatad-Chandler-Garraghan,[21] and others. Recently, Ginzburg[22,23] proposed a phenomenological "two-state, two-(time)scale" (TS2) model which postulated the existence of two separate "states", the low-temperature "Solid" and the high-temperature "Liquid", with both of them characterized by the Arrhenius dependence of the relaxation time on temperature.

The description of the relaxation time (or viscosity) should, ideally, be coupled to the description of the other properties, like specific volume or heat capacity. Here, we concentrate on specific volume. The dependence of specific volume (or density) on temperature and pressure is described by an equation of state (EoS). Those EoS (see, e.g., Rodgers[24]) include variety of empirical (such as the Tait equation[25,26]) and thermodynamic theory-based (Flory-Orwoll-Vrij,[27,28] Prigogine cell model,[29] Dee-Walsh modified cell model,[30,31] Simha-Somcynsky hole model,[32,33] Hartmann-Haque model,[34] Sanchez-Lacombe lattice fluid model,[35–37] and others) approaches. Then, one needs to estimate how the relaxation time couples to the density (or its fluctuations), using approaches like mode-coupling theory (MCT),[38] elastic cooperative nonlinear Langevin equation (ECNLE),[39–42] generalized entropy theory (GET),[43–47] cooperative free volume model,[48–52] "the shoving model",[53] and many others.

Even though there are multiple ways to construct a combined theory for the specific volume and relaxation time, it is important that such a theory satisfy a number of empirically observed constraints. In particular, the dielectric relaxation spectrum often is not a function of the temperature, T, and pressure, P, independently, but rather depends on some combined "state variable" X(T,P),[54] consistent, e.g., with the "coupling model" of Ngai and co-workers.[55] Casalini, Roland, and co-workers determined, in particular, that for many amorphous glass-formers, this constraint can be written in the form of the following scaling relationship, $\tau_\alpha = f(T v_{sp}^{\gamma})$ (where T is temperature and v_{sp} is specific volume).[56–61] Here, the specific volume is calculated based on the temperature and pressure using a parameterized EoS for the liquid state (above the glass transition). The parameter γ is similar to the Grüneisen constant and can be interpreted within a revised entropy theory of glass transition;[56] for polymers, Xu and Freed used

GET to propose a relationship between γ and the polymer bending rigidity, as well as some other molecular parameters.[62] It has been suggested[46,63] that any acceptable theory of glass-forming fluids should have the ability to describe this scaling. (One recent example includes the work of Douglas and Xu[64] in which the Murnaghan EoS[65] was combined with GET).

Very recently, Ginzburg[66,67] formulated a new semi-phenomenological model of glassy materials based on his earlier TS2 dynamic model and the two-state Sanchez-Lacombe EoS.[68,69] The combined model (labeled SL-TS2) was able to capture the Casalini-Roland scaling and correctly describe the α-relaxation time and specific volume vs. temperature for two polymers, polystyrene (PS) and poly(methyl methacrylate) (PMMA). Here, we expand this analysis and apply the model to several other amorphous materials, both low-molecular-weight and polymeric.

The Model and Experimental Methods

The SL-TS2 Model

Thermodynamics – the two-state Sanchez-Lacombe approach

The SL-TS2 (two-state Sanchez-Lacombe) model was described in detail by Ginzburg;[66,67] here, we recap its main features. To begin with, we assume that the glass-forming amorphous material can be separated into small "clusters" or "cooperatively rearranging regions" (CRR). Each CRR might be a single molecule or polymer repeat unit, or a small group of molecules. It is further assumed that the material can exist in one of two states, "Solid" (S) or "Liquid" (L). The "solid" state is characterized by higher density (lower specific volume) and higher zero-temperature cohesive energy density (to be called simply "cohesive energy density" below),

while the "liquid" state has lower density and lower cohesive energy density. Thus, "solid" and "liquid" states have different pressure-volume-temperature (PVT) dependences. Here, we model those dependences using Sanchez-Lacombe (SL) EoS, in which the finite compressibility of the material is modeled by allowing some "lattice sites" to be occupied by "voids" (white squares) with zero mass and zero cohesive energy. Furthermore, we assume that the "solid" CRR has lower volume, i.e., occupies fewer lattice sites as compared to the "liquid" CRR, at any given temperature. Thus, in Figure 1, the "solid" CRR (blue) occupies r_S = 14 lattice sites, and the "liquid" CRR (red) occupies r_L = 20 sites. Also, note that there are more voids in the "liquid" than in the "solid" because of the higher cohesive energy density in the latter. This approach is known as the two-state Sanchez-Lacombe or "Condo model".[68]

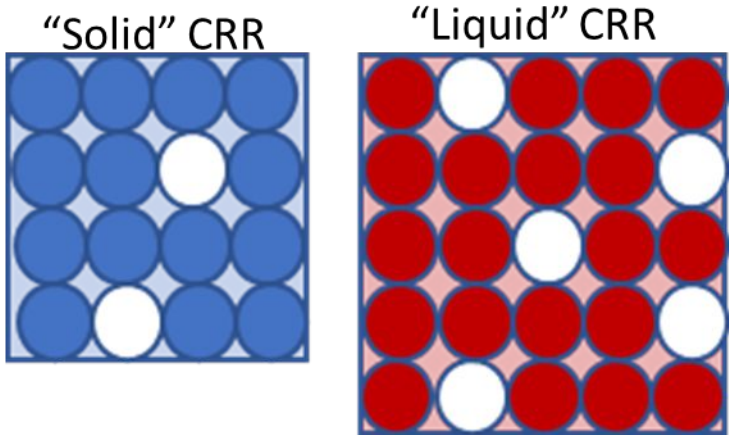

Figure 1. SL-TS2 Model. The voids are shown in white, and the cell size is the same as the void size. In this example, r_S = 14 (the number of non-void cells in the "solid" CRR), and r_L = 20 (the number of non-void cells in the "liquid" CRR).

The free energy of the material is given by,

$$G = k_B T\left[\psi \ln \phi_S + (1-\psi)\ln \phi_L + \langle r\rangle\left\{\frac{1}{\nu}-1\right\}\ln \phi_V\right] \\ -\varepsilon^* \frac{\langle r\rangle}{\nu}\left[\phi_S^2 + 2\alpha_{LS}\phi_L\phi_S + \alpha_{LL}\phi_L^2\right] + \frac{Pv_0\langle r\rangle}{\nu} \quad (1)$$

Here, *P* is the pressure, *T* is the absolute temperature, and k_B is the Boltzmann's constant; ψ is the mole or number fraction of CRRs in the "solid" state, and $\nu = 1 - \phi_V$ is the "occupancy". Other variables in eqn (1) are as follows: ϕ_L, ϕ_S, and ϕ_V are the volume fractions of "liquid", "solid", and void-occupied cells, respectively; v_0 is the volume of one cell (which itself is pressure-dependent). The lattice coordination number is *z*, and the nearest-neighbor interaction energies are ε_{SS}, ε_{SL}, *and* ε_{LL}; the interaction energies including "void" cells are all set to zero, $\varepsilon_{SV} = \varepsilon_{LV} = \varepsilon_{VV} = 0$. We assume the Berthelot "geometric mean" rule, i.e., $\varepsilon_{SL} = (\varepsilon_{SS}\varepsilon_{LL})^{1/2}$. The number of cells occupied by a "liquid cluster" is r_L, and that of the "solid cluster" is r_S; obviously, $r_L > r_S$, so that the liquid density, $\rho_L = \frac{M}{r_L v_0}$, is smaller than the solid density, $\rho_S = \frac{M}{r_S v_0}$ (here, *M* is the mass of the "cluster" or CRR, which is the material constant, independent of T and P). Also, $\langle r\rangle = r_S\psi + r_L(1-\psi)$, $\phi_S = \nu\frac{\psi r_S}{\langle r\rangle}$, $\phi_L = \nu\frac{(1-\psi)r_L}{\langle r\rangle}$, $\phi_V = 1-\nu$, $\alpha_{LS} = \frac{\varepsilon_{LS}}{\varepsilon_{SS}}$, $\alpha_{LL} = \frac{\varepsilon_{LL}}{\varepsilon_{SS}}$, and $\varepsilon^* = \frac{z\varepsilon_{SS}}{2}$. The free energy is minimized with respect to ψ and ν -- see ESI† for more details.

Dielectric Relaxation – the TS2 Model

The "two-state, two-(time)scale" (TS2) model has been proposed in ref.[22] Within this approach, it is stipulated that the characteristic time for "jumps within the cage", τ_1, is the same for both "L" and "S" elements and given by the Arrhenius temperature dependence with

activation energy E_L. The characteristic times for "jumps into neighboring cages", on the other hand, is different for different elements – it is assumed to be equal to τ_1 for jumps between adjacent "L" elements, and equal to a different, larger characteristic time τ_2 for jumps involving at least one "S" element. The characteristic time τ_2 is also postulated to have an Arrhenius temperature dependence with activation energy E_S; in general, $E_S > E_L$. The infinite-temperature limit for both τ_1 and τ_2 is assumed to be the same and labeled τ_∞. (Note that τ_∞, E_S, and E_L are temperature-independent but pressure-dependent). As discussed in ref. [22], the dielectric α- and β (Johari-Goldstein)[70]-relaxation times are given by,

$$\tau_\beta(T,P) \equiv \tau_1(T,P) = \tau_\infty \exp\left[\frac{E_L(P)}{RT}\right] \tag{2a}$$

$$\tau_\alpha(T,P) = \left(\tau_2(T,P)\right)^{\psi(T,P)} \left(\tau_1(T,P)\right)^{1-\psi(T,P)}$$

$$= \tau_\infty \exp\left[\frac{E_L(P)}{RT} + \frac{E_S(P) - E_L(P)}{RT}\psi(T,P)\right] \tag{2b}$$

The eqn (2a) is based on the assumption that the Johari-Goldstein[70] relaxation time is comparable or roughly equal to the "liquid" characteristic time τ_1. The eqn (2b) is an estimate of the α-relaxation time (the time for a particle to diffuse out of its cage) in a mixture of L and S elements based on the effective medium approach (see Supporting Information to ref. [23]) The solid fraction, ψ, obviously depends on the temperature and pressure; however, it can also

depend on the cooling rate or other factors in the non-equilibrium case, as will be discussed below.

As we pointed out in earlier papers,[22,23,66] the α-relaxation as a function of inverse temperature (Arrhenius analysis) can be visualized as a sigmoidal function, with lower slope corresponding to the "L" state, higher slope corresponding to the "S" state, and an abrupt transition between the two asymptotic regions. The center of this transition corresponds to the point where $\psi = 0.5$ (equal balance between "S" and "L"); we denote this temperature as $T_X(P)$. Note that, unlike T_g, T_X is an equilibrium quantity, independent of cooling rate or other experimental conditions.

Equations of evolution for non-equilibrium case (isobaric cooling from equilibrium melt)

To describe the non-equilibrium behavior of ν and ψ during, e.g., cooling from high-temperature equilibrium phase, we used a simple "relaxation time approximation", stipulating[66] that the relaxation time for ψ is the JG β-relaxation and the relaxation time for ν is the (often much slower) α-relaxation, similar in spirit to well-known Tool-Narayanaswami-Moynihan (TNM)[71–73] and Kovacs–Aklonis–Hutchinson–Ramos (KAHR)[74] models. Even further simplification is based on the following assumption (illustrated here for the case $P = 0$ for simplicity, but equally applicable for any P). Let us define T_g ($\geq T_X$) as the temperature below which the temperature change becomes faster than the α-relaxation, i.e., $T_g^{-1}|q|\tau_\alpha\left(T_g\right) \cong 1$ (where $q = \frac{dT}{dt}$ is the cooling rate). In this case, for $T > T_g$, both ψ and ν equilibrate fully, while for $T < T_g$, ν does not change,

while ψ still continues to increase as the temperature is decreased, but significantly slower than in the equilibrium limit. Mathematically, it is expressed as follows,

For $T > T_g$:

$$\nu(T) \equiv \nu_{eq}(T) = F\left(\psi_{eq}(T), T\right) \quad (3a)$$

$$\psi(T) \equiv \psi_{eq}(T) = H\left(\nu_{eq}(T), T\right) \quad (3b)$$

For $T < T_g$:

$$\nu(T) = \nu_{eq}\left(T_g\right) \quad (3c)$$

$$\psi(T) = H\left(\nu_{eq}\left(T_g\right), T\right) \quad (3d)$$

Here, we defined $H(\nu,T)$ as the solution of equation $\frac{\partial G(\psi,\nu;T)}{\partial \psi} = 0$ with respect to ψ; likewise, $F(\psi,T)$ as the solution of equation $\frac{\partial G(\psi,\nu;T)}{\partial \nu} = 0$ with respect to ν; G is the Gibbs free energy defined in *eqn (1).* For more details, see ref.[67] and the ESI†.

The Relaxation-Temperature-Specific Volume (τTV) Scaling

In ref.[67] it was shown that the α-relaxation time as a function of T and P can be written as (see also ESI† for more details),

$$\tau_\alpha(T,P) = f\left[T\left(v_{sp}(T,P)\right)^\gamma\right] = f\left[\frac{T_X(P)}{1+Z}\left(v_{sp,0}(P)\frac{r_S\psi(Z)+r_L\{1-\psi(Z)\}}{r_S\nu(Z)}\right)^\gamma\right]$$

(4)

Here, $Z = \frac{T}{T_X(P)} - 1$ is a "state variable" that combines the effects of temperature and pressure.

To satisfy the Casalini-Roland scaling (the first equal sign), we need to eliminate the explicit pressure dependence in the expression after the second equal sign. This is accomplished if one assumes that all the temperature- and energy-related model parameters scale with pressure as,

$$Y(P) = Y(0)\exp\left(\frac{P}{P_{0,T}}\right) \quad (5a)$$

(here, $Y = T_x, T_g, \varepsilon_{ij}, E_L$, *and* E_S), while the specific volume scales as,

$$v_{sp0}(P) = v_{sp0}(0)\exp\left(-\frac{P}{P_{0,v}}\right) \quad (5b)$$

Here, $P_{0,v} \equiv P^* = B$ is the zero-temperature bulk modulus, and $P_{0,T} = P_{0,v}/\gamma$. This analysis provides an alternative description of the Casalini-Roland parameter γ as the ratio of the bulk modulus *B* and the inverse of the slope of the dependence of $ln(T_g)$ on *P*. For more discussion, see ref.[66] Note that this scaling (eqns (5a) and (5b)) holds only for relatively small pressures, $P << P_{0,T}$; for larger pressures, we expect the specific volume to saturate at some finite value rather than decaying all the way to zero. As will be shown below, $P_{0,T}$ ≥ 1,000 *MPa*, so the SL-TS2 scaling relationships should hold fairly well for pressures up to at least 200 – 300 *MPa*. It is important to note that the Casalini-Roland scaling can extend to significantly larger pressures where eqns (5a) and (5b) are no longer valid and other mechanisms might apply. Another important difference is that the scaling relationships of eqns (5a) and (5b) provide a way to scale

dynamics and specific volume in the glassy state, while the Casalini-Roland scaling has been verified only in the liquid state.

PVT Measurements

In this paper we utilized the specific volume data for eight liquids and polymers: glycerol,[75,76] phenylphthalein-dimethylether (PDE),[77] polychlorinated biphenyls (PCB),[78] o-terphenyl (OTP),[59] polycyclohexylmethacrylate (PCHMA),[79] polyvinylacetate (PVAc),[80,81] polystyrene (PS),[82–84] polymethylmetacrylate (PMMA).[85]

The data reported in this paper have been previously published with a detailed description of the experimental setup. In general, to determine the equation of state (EoS) for glass forming liquids, volume changes are measured as a function of pressure and temperature using a set up like the Gnomix instrument (see, e.g., Zoller and Walsh[86]). A liquid (usually mercury because of its large density) serve as the confining medium, in order to maintain hydrostatic conditions when the sample solidifies by crystallization or vitrification. The differential data are then converted to specific volumes, ν, using the value determined at ambient conditions using the buoyancy method (Archimedes' principle) or helium picnometer. The measurement precision is about 1%.

Dielectric Relaxation Measurements

The relaxation data were taken from earlier publications, as follows: glycerol,[75,76] PDE,[87,88] PCB,[78] OTP,[59,89,90] PCHMA,[79] PVAc,[80,91] PS,[82] PMMA;[85,92] we refer the readers to those

publications for experimental details. In general, typical dielectric measurements are carried out using a parallel plate geometry and the dielectric constant is extracted from impedance measurements performed using impedance analyzers over a broad band of frequency. For measurements at elevated pressure, the sample cell is immersed in a pressure transmitting fluid and contained in a thermalized high pressure Manganin cell, with pressure controlled using hydraulic pumps. Proper choices to isolate the sample cell from the pressure transmitting fluid with small dielectric losses is necessary for accurate measurements. The measurement error is typically 5% or less.

Results and Discussion

The Relaxation Time-Density-Temperature Scaling

Before describing our results in detail, we highlight our approach to the "τTV" scaling. To do this, we use the example relaxation and specific volume data for PDE. Let us consider the relaxation data (Figure 2). The data are collected at various temperatures as a function of the pressure. We collapse all the curves onto a single master curve by introducing the following "effective temperature", T_{eff},

$$T_{eff}\left(T,P\right)=T\exp\left(-\frac{P}{P_{0,T}}\right) \qquad (6)$$

Thus, $T_{eff} = T$ for $P = 0$ (ambient pressure).

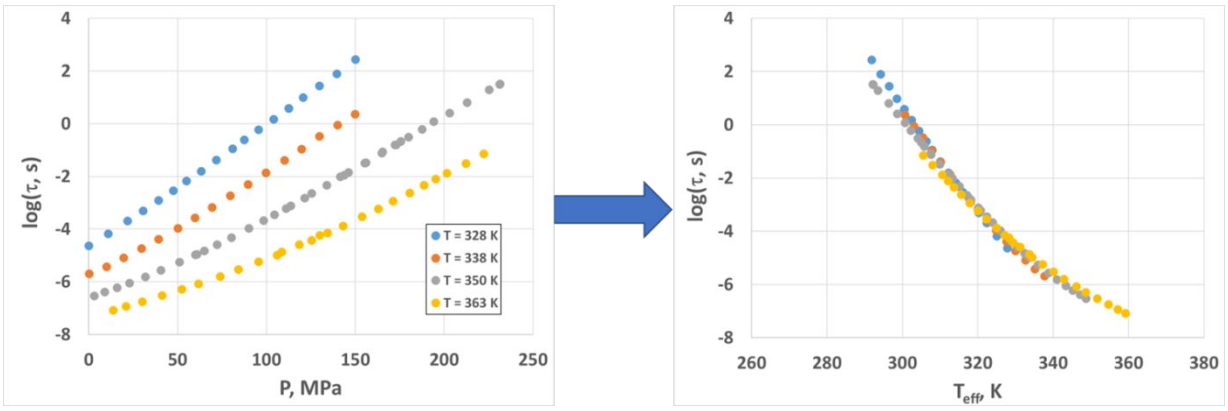

Figure 2. Relaxation time scaling illustration based on PDE data. Left panel – dielectric relaxation time vs. pressure measured for several temperatures. Right panel – same data where the relaxation time is plotted against the effective temperature calculated using eqn (13).

The specific volume data are analyzed in a similar fashion (Figure 3). The temperature axis is scaled according to eqn (6), while the specific volume axis is rescaled in a similar fashion,

$$V_{eff}\left(T,P\right)=v_{sp}\left(T,P\right)\exp\left(\frac{P}{P_{0,V}}\right) \tag{7}$$

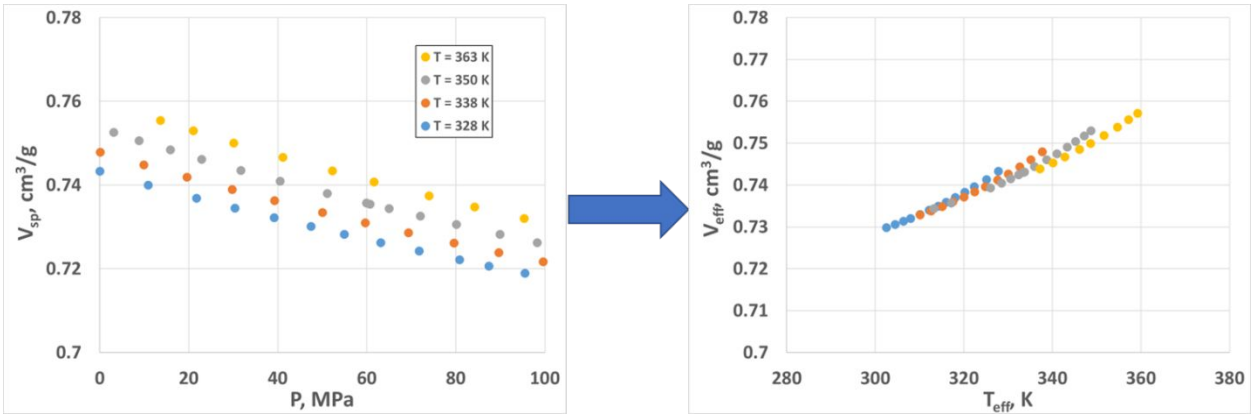

Figure 3. Specific volume scaling illustration based on PDE data. Left panel – specific volume vs. pressure measured for several temperatures. Right panel – same data where the scaled specific volume (eqn (14)) is plotted against the effective temperature (eqn (13)).

The relationship between the two constants $P_{0,V}$ and $P_{0,T}$ is given by,

$$\frac{P_{0,V}}{P_{0,T}} = \gamma \qquad (8)$$

where γ is the Roland-Casalini power-law exponent.[56,58,60] Obviously, the scaling (6) – (7) is approximate and works only for relatively small pressures ($P << P_{0,T} < P_{0,V}$); at higher pressures, the scaling is expected to break down. Even so, given that typically, $P_{0,T} \sim 1$ *GPa*, as we will see below, the SL-TS2 scaling can be used reasonably well for pressures at least up to 200 – 300 *MPa*. The calculated SL-TS2 scaling parameters, $P_{0,T}$ and $P_{0,V}$, are summarized in Table 1 for eight glass-formers, four low-molecular-weight organic and four polymeric, based on the tabulated data from ref. [61] In calculating these parameters, we used eqn (8) and the relationship,

$$\frac{dT_g}{dP} = \frac{T_g\left(P=0\right)}{P_{0,T}} \qquad (9)$$

The parameters $T_g(P=0)$, γ, and dT_g/dP for PDE, OTP, and PCB are regressed based on experimental data; the parameters $P_{0,T}$ and $P_{0,V}$ are then calculated using eqns (8) and (9).[61] The regressed scaling exponent γ for these materials is consistent with estimates of Casalini and Roland,[61] see ESI† for more details.

Table 1. Scaling-related parameters for the eight glass-formers. [61] *"Gly." stands for glycerol. The (absolute) error in T_g is ± 5K, the (relative) error in γ, dT/dP, $P_{0,T}$, and $P_{0,V}$ is approximately 15%.*

Parameter	Units	PDE	PCB	OTP	Gly.	PMMA	PS	PCHMA	PVAc
T_g	K	298	269	246	183	380	353	336	304
γ		4.6	8.5	4.1	1.3	1.8	2.1	2.1	2.5
dT/DP	K/MPa	0.248	0.330	0.246	0.038	0.258	0.328	0.245	0.245
$P_{0,T}$	MPa	1202	815	1000	4816	1473	1076	1371	1241
$P_{0,V}$, MPa	MPa	5527	6929	4050	6261	2651	2260	2880	3102

Below, we will describe the master curves for the same eight glass-formers. The model predictions need to be understood as follows – the figures represent the dielectric relaxation and specific volume vs. temperature for the ambient pressure measurements; the predictions for higher pressures can be obtained using the scaling relationships (6) and (7).

The Parameterization of the Model

Once the master curves are calculated, we can use them to parameterize the SL-TS2 model for each material. The parameterization process is done as follows (below, we set $P = 0$). First, we determine the high-temperature (Arrhenius) activation energy, $E_{L,0}$, and the logarithm of the high-temperature relaxation time, $\log(\tau_\infty)$. Next, we regress all the other parameters; this regression is done using a Monte Carlo process combined with a trial-and-error approach for the selection of initial values. (Note that due to our earlier assumption of the Berthelot geometric mean for the cross-interaction, we automatically have $\alpha_{LS} = \sqrt{\alpha_{LL}}$). The optimization results are summarized in Table 2. For convenience, instead of reporting r_S and r_L, we show $(1/r_{avg}) = 2/(r_S + r_L)$ and $(2\xi) = 2(r_S - r_L)/(r_S + r_L)$; the former is the inverse of the average "chain length", and the latter is the relative volume difference between the "L" and "S" states. Note that if $(1/r_{avg})$ is

sufficiently small, the Sanchez-Lacombe EoS obeys the "corresponding states principle", i.e., all systems with the same reduced temperature and reduced pressure must have the same reduced density.[30,37] Also, the specific volume reported here corresponds to that of the liquid, rather than solid, state. Lastly, note that the glass transition temperature used here is the "dilatometry" T_g which is expected to be slightly different from – though very close to – the DSC or rheology measured T_g. Below, we compare the model fits with experimental data. For more details about the physical meaning of the model parameters and the error estimates, see ESI† and the Discussion section below.

Table 2. SL-TS2 parameters for the eight glass-formers. The parameters are regressed based on the PVT and dielectric relaxation data (see text for details). "Gly." stands for glycerol.

Param.	Units	PDE	PCB	OTP	Gly.	PMMA	PS	PCHMA	PVAc
$\log(\tau_\infty)$		-13.4	-17.4	-13.9	-13.0	-13.0	-12.6	-14.7	-14.6
$E_{L,0}$	kJ/mol	32	50	15	23	35	15	75	35
$E_{S,0}$	kJ/mol	142	160	145	90	213	270	200	186
T*	K	922	761	673	743	918	890	908	740
$V_{spL,0}$	cm^3/g	0.696	0.585	0.881	0.763	0.832	0.940	0.902	0.818
α_{LL}		0.9539	0.9595	0.9515	0.9604	0.9589	0.9589	0.9505	0.9589
$1/r_{avg}$		0.0022	0.0023	0.0032	0.0021	0.0025	0.0025	0.0032	0.0025
(2ξ)		0.046	0.04	0.048	0.04	0.04	0.04	0.048	0.04
$T_{g,model}$, K		292	266	240	180	369	363	370	292

Specific Volume vs. Temperature

In Figure 4, we plot the calculated (lines) vs. measured (symbols) specific volume vs. effective temperature data for the four organic glass-formers (glycerol, ortho-terphenyl, PDE, and PCB-62). For glycerol, we used only the ambient-pressure data, while for the other three materials, multiple-pressure measurements were utilized, as described in the previous section.

Note both good scaling (various datapoints collapse onto a single material-specific master curve) and fair agreement between theory and experiment. Similar to earlier papers,[23,67] here the dashed lines represent the "equilibrium" calculation and the solid lines represent the "constant cooling rate", q ~ 1 K/min, calculation (see previous section for details). For more details, including specific volume vs. pressure plots at various temperatures (PDE, PCB62) and specific volume vs. temperature plots for various pressures (OTP), see ESI†.

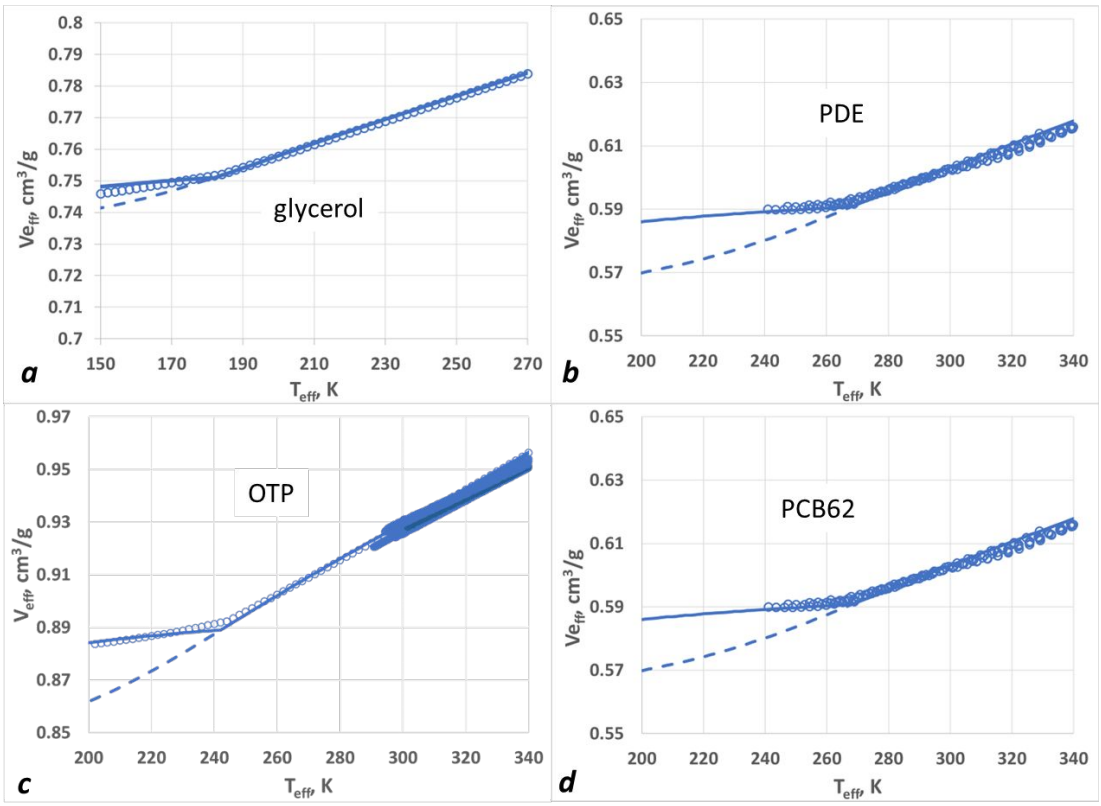

Figure 4. The "effective" specific volume (in cm^3/g) vs. the "effective" temperature (in K) for four low-molecular-weight organic glass-formers: (a) glycerol; (b) PDE; (c) OTP; (d) PCB-62. In all cases, the dashed blue lines are "equilibrium" model and the solid blue lines are "constant cooling rate" model predictions.

Similar behavior can be seen for amorphous polymers (Figure 5). Here, we show only the ambient pressure data and refer the readers to earlier papers on the elevated-pressure behavior.[61] Again, to predict the specific volumes at elevated pressures, one needs to use eqns (6) – (7).

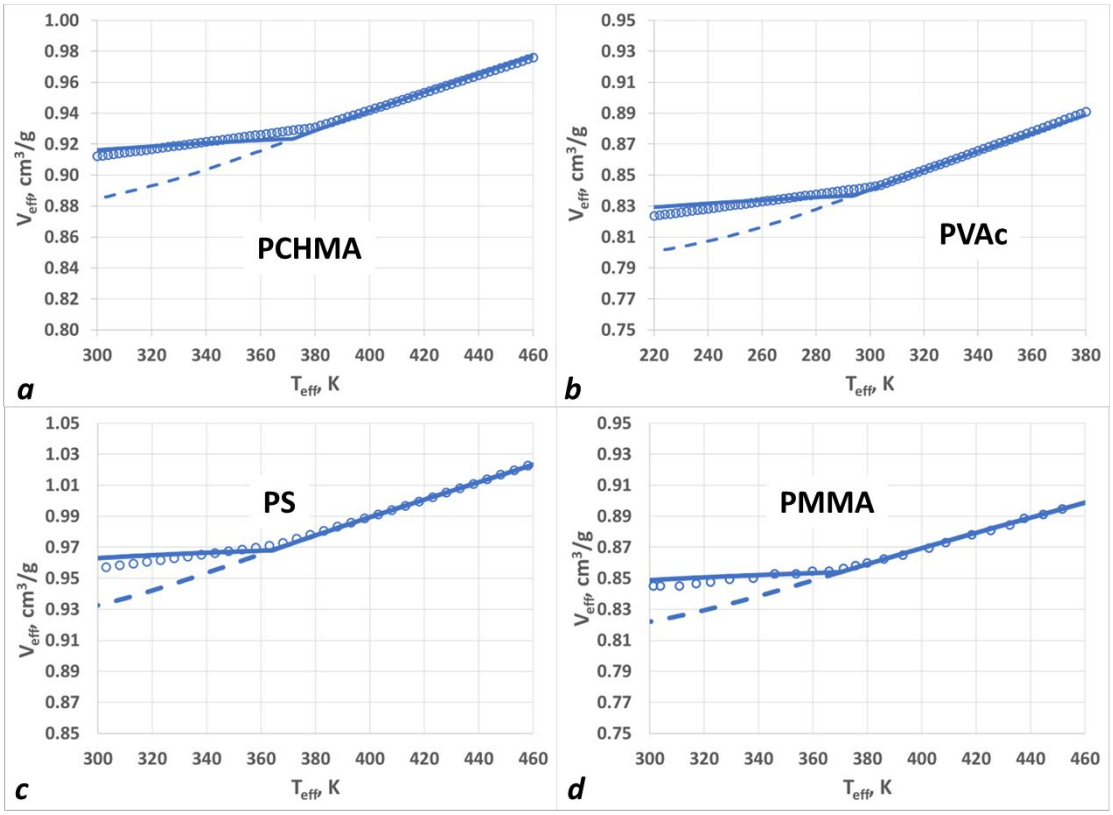

Figure 5. Similar to Figure 4, but for polymeric glass-formers. (a) PCHMA; (b) PVAc; (c) PS; (d) PMMA. (Note that PS and PMMA results were previously published in Ref.[67])

Due to the large number of model parameters, the PVT and relaxation data by themselves might not be sufficient for a unique parameterization, and additional criteria need to be invoked. Here, we attempted to fit the data with an additional constraint (suggested by one of the reviewers) that the CTE above T_g must be a constant or a weakly increasing function of

temperature. Furthermore, for polymers, we considered the observation of Simha and Boyer[93] that the expression $\left(\alpha_l - \alpha_g\right)T_g$ (where α_l and α_g are the coefficients of volumetric thermal expansion in the liquid and glassy states) is approximately a constant, independent of the chemical structure of a polymer. This suggests a thermodynamic similarity between different polymers, so that the purely thermodynamic parameters like α_{LL}, r_{avg}, and 2ξ should be nearly the same, and only the energy scale, T*, should vary. This is indeed what is found (see Table 2). The parameters for non-polymeric glass-formers exhibit larger variation, but still remain within a fairly narrow range.

With the above approach, we generally underestimate the glassy-state CTE. The reason for this is as follows. For the non-equilibrium, real-life cooling, the occupancy ν becomes frozen as T reaches T_g from above. We expect that a more elaborate description of the ν–dynamics would make the transition smoother, reduce the sharpness of the transition and the magnitude of the "downward jump". It is possible, in particular, that the behavior near $T = T_g$ is strongly impacted by the dynamic heterogeneity and relaxation time fluctuations that are not taken into account in the current model. We hope that these improvements will reduce the discrepancy between the model and experiment concerning the glassy CTE.

Dielectric α-Relaxation vs. Temperature

In Figure 6, dielectric α-relaxation data are plotted for the four organic glass-formers. Again, the X-axis is the "effective" temperature, rescaled to the ambient pressure case. The data for OTP, PDE, and PCB are combined from multiple experiments performed at multiple pressures.

Once again, it can be seen that the data collapse well onto single master curves, well-described by the TS2 model.

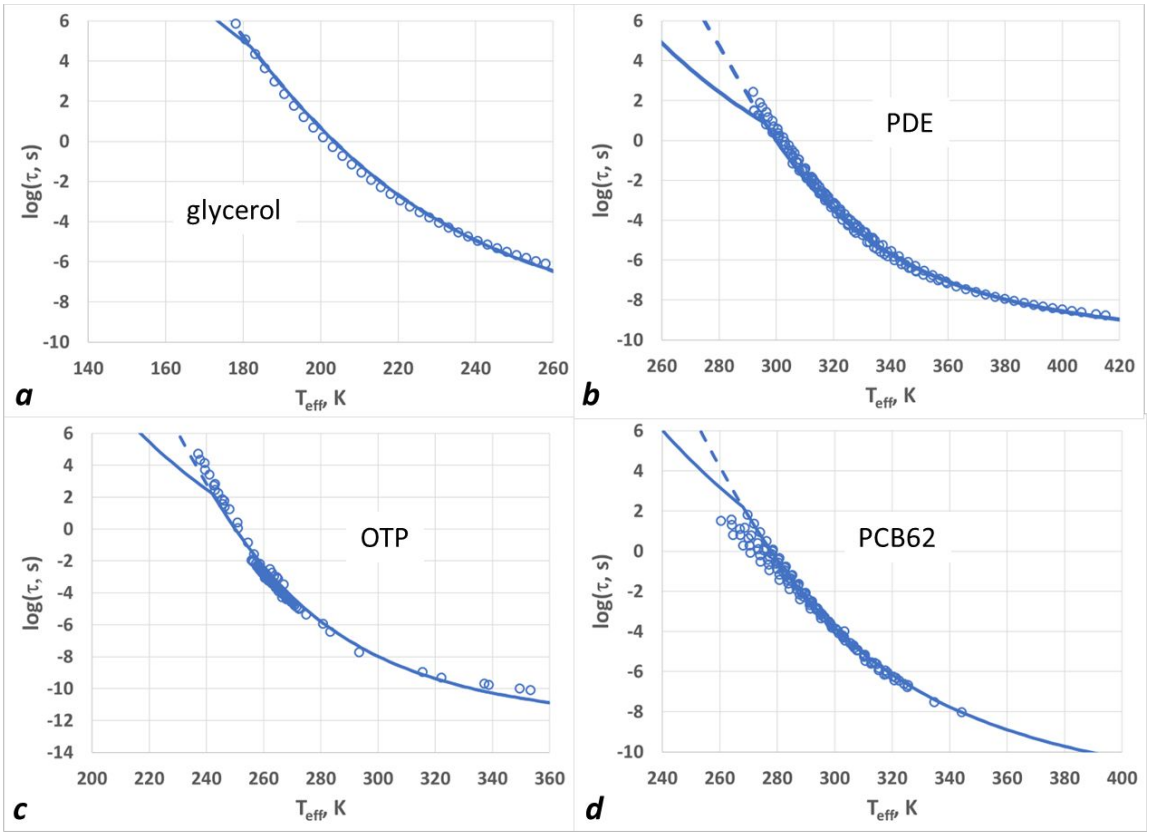

Figure 6. Logarithm of the α-relaxation time as a function of the "effective" temperature for the four organic glass-formers: (a) glycerol, (b) PDE, (c) ortho-terphenyl, and (d) PCB. The symbols are experimental data (see text for more details), the dashed lines are "equilibrium" predictions, and the solid lines are the "constant cooling rate" predictions.

Figure 7 shows the same comparison (TS2 model vs. dielectric relaxation data) for the four polymeric glass-formers (PMMA, PS, PCHMA, and PVAc). Again, we use only the ambient pressure data, but given that the τTV scaling has been shown to work for all of these polymers, we expect

that the model should be able to predict the higher-pressure relaxation with the help of simple temperature rescaling (eqn (6)).

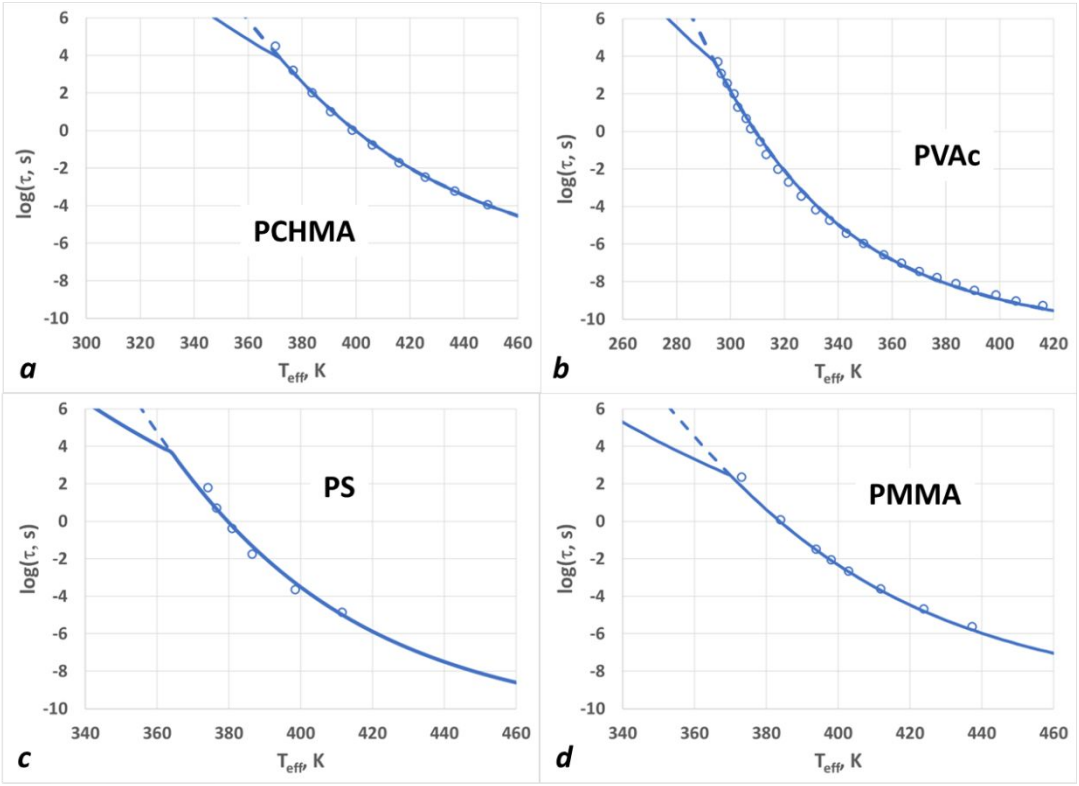

Figure 7. Same as in Figure 6, but for the four polymeric glass-formers. (a) PCHMA, (b) PVAc, (c) PS, and (d) PMMA.

The fact that the dielectric relaxation time data are closer to the equilibrium calculation than the specific volume data is not surprising. The specific volume data are measured at constant pressure cooling the sample at a constant cooling rate typically 0.5 – 1 K/min, while the dielectric relaxation measurements are performed waiting for long equilibration times during cooling or compression that are typically of the order or 0.5 – 1 hr. Thus, the samples have

significantly more time to equilibrate during the dielectric measurements than during the specific volume measurements.

Discussion

We have expanded our earlier work on modeling dielectric relaxation and PVT in organic and polymeric glass-formers using SL-TS2 approach. To begin with, we showed that SL-TS2 is naturally compatible with the Casalini-Roland thermodynamical scaling, so that both density-temperature and relaxation time-temperature data collected at various pressures can be collapsed onto unique material-dependent master curves. Next, we showed that those master curves can be successfully described by the SL-TS2 equations, and summarized thermodynamic and relaxation dynamic parameters for the eight glass-formers studied here. The SL-TS2 allows the extension of the scaling in the glass state, while the Casalini-Roland thermodynamical scaling has been demonstrated only in the liquid phase.

The SL-TS2 model parameters are related to specific experimentally measured parameters, such as the coefficients of thermal expansion in glassy and liquid states, the specific volume at $T = T_g$, the activation energy in the high-temperature Arrhenius regime, the limiting high-temperature relaxation time, the temperature corresponding to the transition from VFTH to Arrhenius, and the two VFTH parameters related to the fragility and the apparent relaxation time divergence temperature. Thus, in principle, SL-TS2 has the same number of independent parameters as there are potential “degrees of freedom” in the experimental data. However, in many cases, the high-temperature Arrhenius region is fully or partially inaccessible, and thus the

SL-TS2 parameter determination becomes less accurate (see ESI† for more detail). On the other hand, the same region can be readily investigated using atomistic or coarse-grained Molecular Dynamics (MD) simulations.[94] Thus, in principle, SL-TS2 (or similar) approach offers an interesting opportunity to combine experimental results (moderate characteristic times, ~10^{-6} – 10^{3} s) with simulation data (small characteristic times, ~10^{-12} – 10^{-6} s). We plan to further explore the physical meaning of the SL-TS2 parameters in the future, as well as investigate other possible equations of state (EoS)[27,28,30–33,95,96] in place of Sanchez-Lacombe. Another way to test and potentially improve the theory and parameterization is to model the volume relaxation following the "up" and "down" temperature jumps,[74,82,85,97] which is a subject of ongoing research. As already pointed out, additional considerations, such as the Simha-Boyer rule[93] or the requirement that the liquid-state CTE must be a constant or a weakly increasing function of temperature, can be used to reduce the parameterization uncertainty. Note that the last condition results from an interesting interplay of two factors – the coefficient of thermal expansion above T_g is the sum of the Sanchez-Lacombe contribution, $-d\ln(v)/dT$, which is weakly increasing with temperature, and the two-state balance contribution, $d\ln(\langle r \rangle)/dT$, which is decreasing with temperature. One thus expects the total CTE to depend strongly on the chosen EoS.

For polymeric materials, the material properties depend strongly on molecular weight, especially for relatively short polymers (M < 10,000 g/mol).[1,98–103] Here, we consider only the high-molecular weight limit (M > 100,000 g/mol). In principle, the SL-TS2 parameters for polymers should be molecular-weight-dependent, in the same way as VFTH or WLF parameters are. This will be another topic for future studies.

Conclusions

We applied the SL-TS2 (two-state Sanchez-Lacombe) framework to describe PVT and dielectric α-relaxation data for eight amorphous glass-forming materials (four organic and four polymeric). For all these materials, the dielectric and PVT data were previously shown to obey the Casalini-Roland scaling, $\tau_\alpha = f(Tv_{sp}^{\gamma})$. Here, we first utilized the two-state SL-TS2 framework to successfully describe the dielectric relaxation and the volumetric thermal expansion for all these glass-formers at ambient pressure. Next, we showed that the Casalini-Roland scaling emerges naturally within SL-TS2, provided that the "units" of energy and density are all rescaled appropriately with pressure. The resulting model fits for the relaxation time and specific volume can be applied for low and moderate (up to ~200 MPa) pressures extending also in the glassy state.

Conflicts of Interest

There are no conflicts of interest to declare.

Acknowledgments

We thank anonymous reviewers for many helpful comments and suggestions. R.C. acknowledges the support of the Office of Naval Research (N0001421WX00833-B).

References

1 J. Bicerano, *Prediction of polymer properties*, CRC Press, Boca Raton, FL, 3rd ed., 2002.

2 C. B. Roth, *Polymer glasses*, CRC Press, 2016.

3 G. B. McKenna and S. L. Simon, *Macromolecules*, 2017, **50**, 6333–6361.

4 C. A. Angell, *Curr Opin Solid State Mater Sci*, 1996, **1**, 578–585.

5 C. A. Angell, *Encyclopedia of materials: Science and technology*, 2001, **4**, 3365.

6 A. Zaccone and E. M. Terentjev, *Phys Rev Lett*, 2013, **110**, 178002.

7 D. W. van Krevelen and K. te Nijenhuis, *Properties of polymers: their correlation with chemical structure; their numerical estimation and prediction from additive group contributions*, Elsevier, Amsterdam, 4th ed., 2009.

8 D. Cangialosi, *Journal of Physics: Condensed Matter*, 2014, **26**, 153101.

9 D. Cangialosi, A. Alegria and J. Colmenero, *Prog Polym Sci*, 2016, **54**, 128–147.

10 L. Berthier and M. D. Ediger, *Phys Today*, 2016, **69**, 40–46.

11 M. D. Ediger, C. A. Angell and S. R. Nagel, *J Phys Chem*, 1996, **100**, 13200–13212.

12 H. Vogel, *Phys. Z.*, 1921, **22**, 645–646.

13 G. S. Fulcher, *Journal of the American Ceramic Society*, 1925, **8**, 339–355.

14 G. Tammann and W. Hesse, *Z. Anorg. Allg. Chem*, 1926, **156**, 245–257.

15 M. L. Williams, R. F. Landel and J. D. Ferry, *J Am Chem Soc*, 1955, **77**, 3701–3707.

16 A. K. Doolittle, *J Appl Phys*, 1951, **22**, 1471–1475.

17 G. Adam and J. H. Gibbs, *J Chem Phys*, 1965, **43**, 139–146.

18 J. C. Mauro, Y. Yue, A. J. Ellison, P. K. Gupta and D. C. Allan, *Proceedings of the National Academy of Sciences*, 2009, **106**, 19780–19784.

19 J. Krausser, K. H. Samwer and A. Zaccone, *Proceedings of the National Academy of Sciences*, 2015, **112**, 13762–13767.

20 I. Avramov and A. Milchev, *J Non Cryst Solids*, 1988, **104**, 253–260.

21 Y. S. Elmatad, D. Chandler and J. P. Garrahan, *J Phys Chem B*, 2010, **114**, 17113–17119.

22 V. Ginzburg, *Soft Matter*, 2020, **16**, 810–825.

23 V. Ginzburg, *Macromolecules*, 2021, **54**, 2774–2782.

24 P. A. Rodgers, *J Appl Polym Sci*, 1993, **48**, 1061–1080.

25 J. H. Dymond and R. Malhotra, *Int J Thermophys*, 1988, **9**, 941–951.

26 R. Y. Chang, C. H. Chen and K. S. Su, *Polym Eng Sci*, 1996, **36**, 1789–1795.

27 P. J. Flory, R. A. Orwoll and A. Vrij, *J Am Chem Soc*, 1964, **86**, 3507–3514.

28 P. J. Flory, R. A. Orwoll and A. Vrij, *J Am Chem Soc*, 1964, **86**, 3515–3520.

29 I. Prigogine, A. Bellemans and V. Mathot, *Solutions, North-Holland, Amsterdam*.

30 G. T. Dee and D. J. Walsh, *Macromolecules*, 1988, **21**, 811–815.

31 G. T. Dee and D. J. Walsh, *Macromolecules*, 1988, **21**, 815–817.

32 R. Simha and T. Somcynsky, *Macromolecules*, 1969, **2**, 342–350.

33 G. A. Carri, *Chinese Journal of Polymer Science*, 2015, **33**, 523–539.

34 B. Hartmann and M. A. Haque, *J Appl Polym Sci*, 1985, **30**, 1553–1563.

35 R. H. Lacombe and I. C. Sanchez, *J Phys Chem*, 1976, **80**, 2568–2580.

36 I. C. Sanchez and R. H. Lacombe, *Macromolecules*, 1978, **11**, 1145–1156.

37 I. C. Sanchez and R. H. Lacombe, *J Phys Chem*, 1976, **80**, 2352–2362.

38 L. M. C. Janssen, *Front Phys*, 2018, **6**, 97.

39 S. Mirigian and K. S. Schweizer, *J Chem Phys*, 2014, **140**, 194506.

40 S. Mirigian and K. S. Schweizer, *J Chem Phys*, 2014, **140**, 194507.

41 A. D. Phan and K. S. Schweizer, *Journal of Physical Chemistry B*, 2018, **122**, 8451–8461.

42 A. D. Phan and K. S. Schweizer, *Macromolecules*, 2018, **51**, 6063–6075.

43 J. Dudowicz, K. F. Freed and J. F. Douglas, *Adv Chem Phys*, 2008, **137**, 125.

44 W. S. Xu, J. F. Douglas and K. F. Freed, *Adv Chem Phys*, 2016, **161**, 443–497.

45 E. B. Stukalin, J. F. Douglas and K. F. Freed, *Journal of Chemical Physics*, 2009, **131**, 114905.

46 W.-S. Xu, J. F. Douglas and Z.-Y. Sun, *Macromolecules*, 2021, **54**, 3001–3033.

47 W.-S. Xu, J. F. Douglas, W. Xia and X. Xu, *Macromolecules*, 2020, **53**, 7239–7252.

48 R. P. White and J. E. G. Lipson, *Macromolecules*, 2016, **49**, 3987–4007.

49 R. P. White and J. E. G. Lipson, *J Chem Phys*, 2017, **147**, 184503.

50 R. P. White and J. E. G. Lipson, *Macromolecules*, 2018, **51**, 7924–7941.

51 R. P. White and J. E. G. Lipson, *The European Physical Journal E*, 2019, **42**, 100.

52 R. P. White and J. E. G. Lipson, *ACS Macro Lett*, 2017, **6**, 529–534.

53 J. C. Dyre, T. Christensen and N. B. Olsen, *J Non Cryst Solids*, 2006, **352**, 4635–4642.

54 K. L. Ngai, R. Casalini, S. Capaccioli, M. Paluch and C. M. Roland, *J Phys Chem B*, 2005, **109**, 17356–17360.

55 K. L. Ngai, *J Chem Phys*, 1998, **109**, 6982–6994.

56 R. Casalini and C. M. Roland, *Phys Rev E*, 2004, **69**, 62501.

57 R. Casalini, U. Mohanty and C. M. Roland, *J Chem Phys*, 2006, **125**, 14505.

58 C. M. Roland, S. Bair and R. Casalini, *J Chem Phys*, 2006, **125**, 124508.

59 R. Casalini, S. S. Bair and C. M. Roland, *J Chem Phys*, 2016, **145**, 64502.

60 C. M. Roland, S. Hensel-Bielowka, M. Paluch and R. Casalini, *Reports on Progress in Physics*, 2005, **68**, 1405.

61 R. Casalini and C. M. Roland, *Phys Rev Lett*, 2014, **113**, 85701.

62 W.-S. Xu and K. F. Freed, *J Chem Phys*, 2013, **138**, 234501.

63 N. Gnan, T. B. Schrøder, U. R. Pedersen, N. P. Bailey and J. C. Dyre, *J Chem Phys*, 2009, **131**, 234504.

64 J. F. Douglas and W.-S. Xu, *Macromolecules*, 2021, **54**, 3247–3269.

65 F. D. Murnaghan, *Proceedings of the National Academy of Sciences*, 1944, **30**, 244–247.

66 V. Ginzburg, *Soft Matter*, 2021, **17**, 9094–9106.

67 V. Ginzburg, *Macromolecules*, 2022, **55**, 873–882.

68 P. D. Condo, I. C. Sanchez, C. G. Panayiotou and K. P. Johnston, *Macromolecules*, 1992, **25**, 6119–6127.

69 H. Alam, C. B. Park and R. B. Thompson, *Polymer (Guildf)*, 2020, 123334.

70 G. P. Johari and M. Goldstein, *J Chem Phys*, 1970, **53**, 2372–2388.

71 A. Q. Tool, *Journal of the American Ceramic society*, 1946, **29**, 240–253.

72 O. Narayanaswamy, *Journal of the American Ceramic Society*, 1971, **54**, 491–498.

73 C. T. Moynihan, P. B. Macedo, C. J. Montrose, C. J. Montrose, P. K. Gupta, M. A. DeBolt, J. F. Dill, B. E. Dom, P. W. Drake and A. J. Easteal, *Ann N Y Acad Sci*, 1976, **279**, 15–35.

74 A. J. Kovacs, J. J. Aklonis, J. M. Hutchinson and A. R. Ramos, *Journal of Polymer Science: Polymer Physics Edition*, 1979, **17**, 1097–1162.

75 G. P. Johari and E. Whalley, *Faraday Symposia of the Chemical Society*, 1972, **6**, 23–41.

76 M. Paluch, R. Casalini, S. Hensel-Bielowka and C. M. Roland, *J Chem Phys*, 2002, **116**, 9839–9844.

77 R. Casalini, M. Paluch, J. J. Fontanella and C. M. Roland, *J Chem Phys*, 2002, **117**, 4901–4906.

78 C. M. Roland and R. Casalini, *J Chem Phys*, 2005, **122**, 134505.

79 C. M. Roland and R. Casalini, *Macromolecules*, 2007, **40**, 3631–3639.

80 C. M. Roland and R. Casalini, *Macromolecules*, 2003, **36**, 1361–1367.

81 J. E. McKinney and R. Simha, *Macromolecules*, 1974, **7**, 894–901.

82 L. Grassia and S. L. Simon, *Polymer (Guildf)*, 2012, **53**, 3613–3620.

83 R. Tao and S. L. Simon, *J Polym Sci B Polym Phys*, 2015, **53**, 1131–1138.

84 X. Zhao, L. Grassia and S. L. Simon, *Macromolecules*, 2021, **54**, 8352–8364.

85 L. Grassia and A. D'Amore, *J Non Cryst Solids*, 2011, **357**, 414–418.

86 D. Walsh and P. Zoller, *Standard Pressure Volume Temperature Data for Polymers*, Taylor & Francis, 1995.

87 M. Paluch, C. M. Roland, R. Casalini, G. Meier and A. Patkowski, *J Chem Phys*, 2003, **118**, 4578–4582.

88 M. Paluch, R. Casalini, A. Best and A. Patkowski, *J Chem Phys*, 2002, **117**, 7624–7630.

89 J. M. Caruthers and G. A. Medvedev, *Phys Rev Mater*, 2018, **2**, 55604.

90 J. C. Yungbluth, G. A. Medvedev, B. M. Savoie and J. M. Caruthers, *J Chem Phys*, 2020, **152**, 94504.

91 W. Heinrich and B. Stoll, *Colloid Polym Sci*, 1985, **263**, 873–878.

92 S. Theobald, W. Pechhold and B. Stoll, *Polymer (Guildf)*, 2001, **42**, 289–295.

93 R. Simha and R. F. Boyer, *J Chem Phys*, 1962, **37**, 1003–1007.

94 J.-H. Hung, T. K. Patra, V. Meenakshisundaram, J. H. Mangalara and D. S. Simmons, *Soft Matter*, 2019, **15**, 1223–1242.

95 D. J. Walsh and G. T. Dee, *J Supercrit Fluids*, 1989, **2**, 57–62.

96 M. Wang, S. Takishima, Y. Sato and H. Masuoka, *Fluid Phase Equilib*, 2006, **242**, 10–18.

97 S. L. Simon, J. W. Sobieski and D. J. Plazek, *Polymer (Guildf)*, 2001, **42**, 2555–2567.

98 B. Schmidtke, M. Hofmann, A. Lichtinger and E. A. Rössler, *Macromolecules*, 2015, **48**, 3005–3013.

99 D. L. Baker, M. Reynolds, R. Masurel, P. D. Olmsted and J. Mattsson, *Phys Rev X*, 2022, **12**, 21047.

100 V. N. Novikov and A. P. Sokolov, *Nature*, 2004, **431**, 961–963.

101 V. N. Novikov and A. P. Sokolov, *Phys Rev E*, 2003, **67**, 31507.

102 A. L. Agapov and A. P. Sokolov, *Macromolecules*, 2009, **42**, 2877–2878.

103 K. Kunal, C. G. Robertson, S. Pawlus, S. F. Hahn and A. P. Sokolov, *Macromolecules*, 2008, **41**, 7232–7238.

TOC Graphics